Nanoparticle-Shelled Catalytic Bubble Micromotor

Laura L. A. Adams, Daeyeon Lee,* Yongfeng Mei, David A. Weitz, and Alexander A. Solovev*

Nanoparticle-shelled bubbles, prepared with glass capillary microfluidics, are functionalized to produce catalytic micromotors that exhibit novel assembly and disassembly behaviors. Stable microbubble rafts are assembled at an air–solvent interface of nonaqueous propylene carbonate (PC) solvent by creating a meniscus using a glass capillary. Upon the addition of hydrogen peroxide fuel, catalytic microbubbles quickly break free from the bubble raft by repelling from each other and self-propelling at the air–fuel interface (a mixture of PC and aqueous hydrogen peroxide). While most of micromotors generate oxygen bubbles on the outer catalytic shell, some micromotors contain cracks and eject bubbles from the hollow shells containing air. Nanoparticle-shelled bubbles with a high buoyancy force are particularly attractive for studying novel propulsion modes and interactions between catalytic bubble micromotors at air–fuel interfaces.

Chemically triggered, externally powered, and artificially fabricated micromotors, engines, rotors, and pumps have shown a wide range of propulsion schemes, speeds, and chemomechanical responses leading to a wide variety of potential applications.[1] Similar to the spontaneous motility of cells and motor proteins, nano/micromachines are capable of converting chemical energy to mechanical energy to propel themselves in various fluids.[2] Several viable motive mechanisms have been identified outside the realm of biological motility such as self-electrophoresis, self-diffusiophoresis, dynamic surface/interfacial tension, and bubble recoiling.[3] Moreover, it is widely believed that micro- and nanomachines can address and solve numerous challenges involving transport,

Dr. L. L. A. Adams, Prof. D. A. Weitz, Prof. A. A. Solovev
Gordon McKay Laboratory
Harvard University
Oxford St., Cambridge, MA 02138, USA
Dr. L. L. A. Adams
Department of Physics and Astronomy
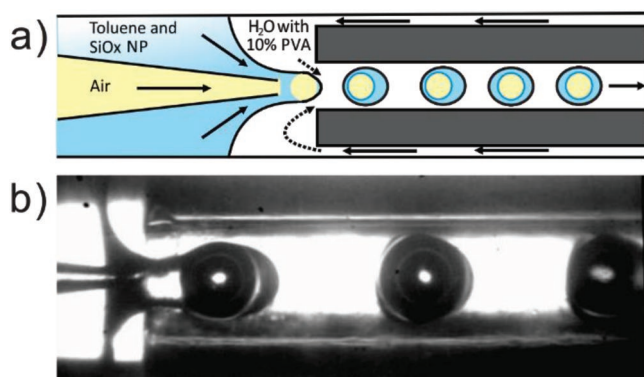University of Minnesota-Duluth
Duluth, MN 55812, USA
Prof. D. Lee
Department of Chemical and Biomolecular Engineering
University of Pennsylvania
Philadelphia, PA 19104, USA
E-mail: daeyeon@seas.upenn.edu
Prof. Y. F. Mei, Prof. A. A. Solovev
Materials Science Department
Fudan University
220 Handan Road, Shanghai 200433, P. R. China
E-mail: solovev@fudan.edu.cn

assembly of cargo payloads,[4] delivery of drugs,[5,6] analytical chemistry,[7] water treatment,[8–10] and oil removal,[11,12] to name a few examples. However, micromotors typically consist of materials whose density and weight are higher than that of the liquids they are dispersed in, causing the micromachines to sediment and sink in the media. In natural aquatic environments, such as deep rivers and lakes, these sinking micromotors can deleteriously affect the environment by causing pollution and environmental hazards. In contrast, buoyant micromotors can be easily removed from the air–water interface after accomplishing their operation, minimizing their environmental impact. To date, several approaches have been designed to fabricate lightweight micromotors with ultra-thin shells. Thin-shelled micromotors include rolled-up inorganic nanomembranes,[13,14] etched spherical particles,[15] trimetallic microcaps,[16] layer-by-layer assembled polyelectrolyte multilayer hollow capsules,[17] and Janus-like vesicular motors with catalyst-containing membrane.[18] However, missing in this research area, are investigations of gas-cored micromotors with a permanent buoyancy force. Moreover, the next important area of research in this field is the realization of active swimmers that can autonomously sense, interact, and assemble to achieve dynamic self-assembly.[19,20] For swarming, collective behaviors with contactless short- and long-range interactions among active particles must be considered,[21,22] which can be modulated by light,[23,24] magnetic,[25] and acoustic[26] fields.

In this study, we report a new type of gas-cored micromotors, which are intrinsically buoyant in liquids. These micromotors have thin shells made of silica nanoparticles and are half-coated with a Ti/Pt catalyst. We take advantage of recent methods of producing stable air/oil/water compound bubbles by glass capillary microfluidics.[27] Gas-cored bubbles with nanoparticle-decorated stable shells have unique properties such as being lightweight, having a high buoyancy, a mechanically robust structure that can withstand drying and materials deposition in vacuum. When placed through the interface between air and propylene carbonate (PC), an external glass capillary attracts and produces a raft of catalytic nanoparticle-shelled bubbles. Upon the addition of H_2O_2 fuel in PC, catalytic bubble micromotors (CBMs) convert H_2O_2 into oxygen bubbles and water, repel each other, and break free from the microbubble raft, self-propelling across the air–fuel interface.

We produce highly buoyant catalytic micromotors consisting of nanoparticle-shelled microbubbles with coated Ti/Pt

**ADVANCED
SCIENCE NEWS**
www.advancedsciencenews.com

**ADVANCED
MATERIALS
INTERFACES**
www.advmatinterfaces.de

Figure 1. Generation of air-in-oil-in-water compound microbubbles using glass capillary microfluidic device. a) Schematic illustration of a glass capillary microfluidic device, where air is injected in the inner capillary and toluene containing silica nanoparticles is injected in the space between the inner and outer capillaries. The air–water interface is stabilized by the formation of a nanoparticle shell. Poly vinyl alcohol (10%, PVA) is used to avoid agglomeration of bubbles. b) Optical microscopy image showing the process of gas encapsulation and the formation of monodisperse nanoparticle-shelled bubbles.

layers (Supporting Information). The CBM production process begins with the microfluidic generation of encapsulated bubbles inside the nanoparticle shells,[27,28] as depicted in the schematic of **Figure 1**a,b. Following the techniques outlined in a previous report,[27] we use a commercially available solution of silica nanoparticles dispersed in toluene for the formation of the shell. In the microfluidic generation of these compound microbubbles, this solvent is the middle phase and the pressurized
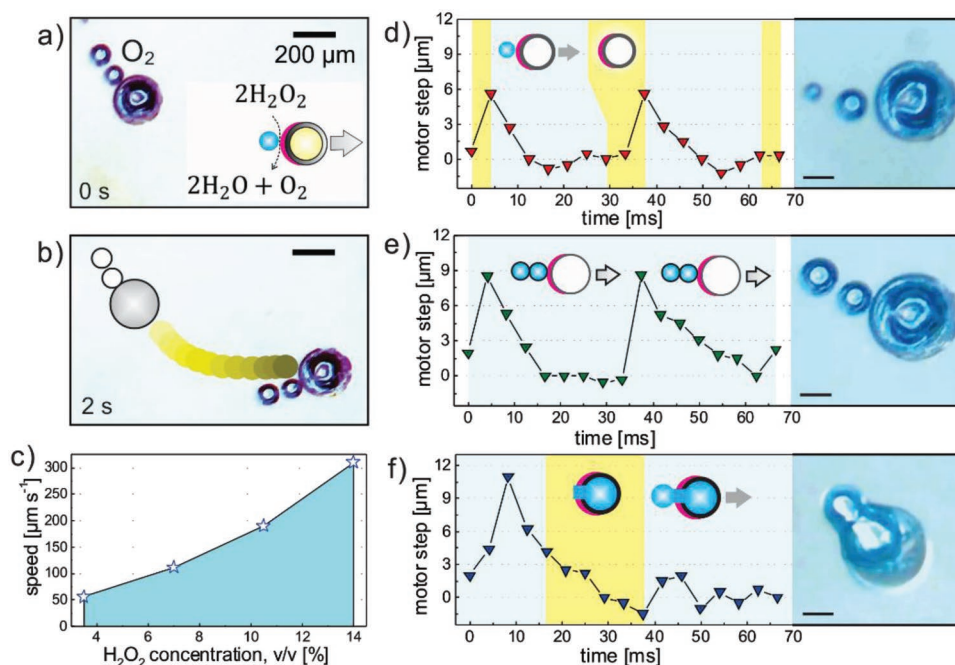
air is sent through the bore of the injection capillary, as shown in the schematic of Figure 1a.

A schematic drawing of the process, where silica nanoparticles assemble around bubble, is shown in **Figure 2**a. Optical microscopy images corresponding to bubbles drying during the 28 days are illustrated in Figure 2b. As the toluene evaporates, the silica nanoparticles move to the interface, stabilizing the bubble, and forming a very rigid shell. Scanning electron microscopy (SEM) image shows an assembly of dry microbubbles with an average diameter of 170 μm, Figure 2c. As toluene evaporates, the shell becomes smaller in size and stiffer. The diameter change in time is shown in Figure 2d (different sample from Figure 2c). An average shell thickness of 3.1 μm is measured by slicing the shell of a microbubble with a razor blade as seen in the SEM image in the inset of Figure 2d. A schematic drawing and a stereo microscopy image of microbubbles with evaporated titanium/platinum Ti/Pt layers are provided in Figure 2e,f. In the last step, the encapsulated bubbles are rinsed in isopropanol, dried on a solid surface and coated with Ti/Pt layers using an e-beam evaporator. The titanium is used as a wetting layer.

Bubbles are stored in the liquid, the SiO_2 nanoparticles are hydrophobic and water does not infiltrate through the shells. The shell structure remains intact without collapsing and there could be exchange of air between the inside and outside for thin shell structures. Moreover, due to a high buoyancy the encapsulated bubbles remain intact at the air–water interface. When placed in hydrogen peroxide fuel, oxygen bubbles are generated i) on catalytic surface of Janus Ti/Pt-SiO_2 bubbles or ii) from the gas core through an opening or a defect in the micromotor shell. It is observed that some fraction of
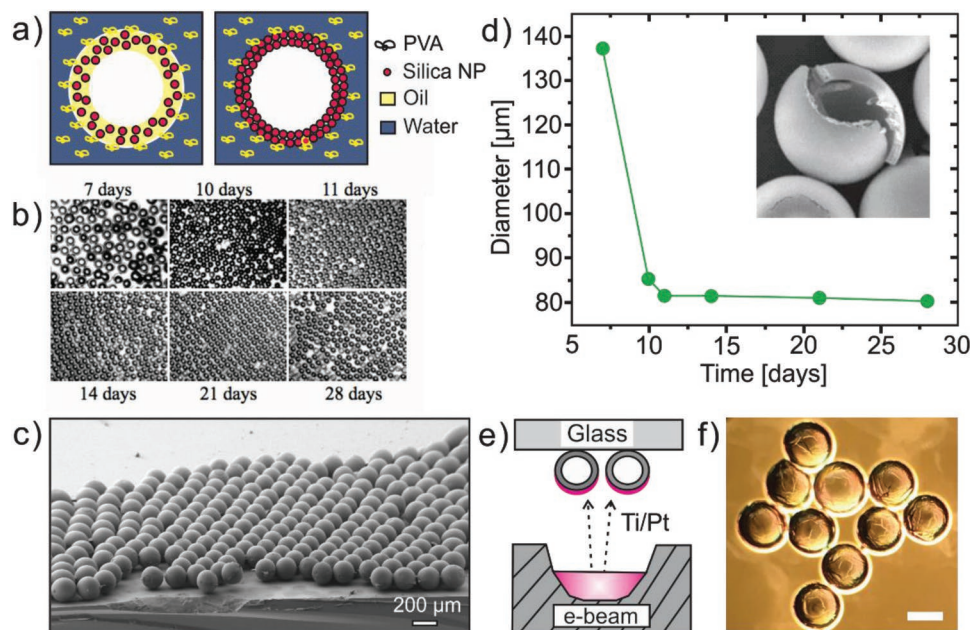
Figure 2. Fabrication of nanoparticle-shelled CBMs using microfluidics and e-beam deposition. a) A schematic of the bubble drying process: evaporation of oil leads to mechanical stabilization of the bubble shell. b) Optical microscopy images of microbubbles dried during 28 days. c) An SEM image of silica nanoparticle-shelled microbubbles. d) An observed reduction of the bubble diameter from 138 to 78 μm during 28 days. e) Schematic of electron-beam evaporation of Ti/Pt layers on SiO_2 microbubbles in vacuum using e-beam. f) Optical microscopy image of coated SiO_2/Ti/Pt microbubbles. The scale bar is 100 μm.

ADVANCED
SCIENCE NEWS
www.advancedsciencenews.com

ADVANCED
MATERIALS
INTERFACES
www.advmatinterfaces.de

Figure 3. Propulsion mechanisms of micromotors in the mixture of PC and hydrogen peroxide. a,b) Tracked trajectory of motion showing a trajectory of an individual CBM during 2 s. c) Characterization of CBMs' speed in different concentrations of H_2O_2 fuel. d–f) Analysis of micromotors motion driven by d) the single bubble, e) double bubbles, and f) the bubble generated from the internally stored gas core. The scale bar is 50 µm.

nanoparticle-shelled microbubbles have holes/openings developed during drying step before e-beam deposition. A deposition of platinum catalyst in the interior of the damaged shell is not required for an ejection of oxygen bubbles from the hollow shells containing air. Gas pockets can provide a sustainable generation of microbubbles if a supply of gas molecules is continuously provided.[29] The CBMs are powered by the catalytic reaction $2H_2O_2 \rightarrow 2H_2O + O_2$. A typical trajectory of an individual micromotor in the mixture of hydrogen peroxide (5% v/v H_2O_2), water, and PC during a time interval of 2 s is shown in **Figure 3**a,b. A dependence of micromotors' speed in different concentrations of H_2O_2 fuel is shown in Figure 3c. As expected, CBMs' speed increases in solutions containing higher concentrations of hydrogen peroxide. Individual CBMs swim in three distinct modes: i) a single bubble generated on the surface of the Pt-coated shell, ii) a single bubble ejected from the internal gas core, and iii) a collision between the O_2 bubbles, leading to a double bubbles trains (Video S1, Supporting Information). The displacement of an individual CBM self-propelled by the recoil of a single O_2 bubble is shown in Figure 3d. In the latter case, the O_2 bubble nucleates, grows, and bursts on the outer surface of the nanoparticle shell, leading to an average step of 5 µm. As a result, the O_2 gas bubble is connected to the CBM for approximately 20 ms (i.e., motor-bubble interaction time, indicated as a blue region on the graph). After the O_2 bubble is detached, during next 10 ms (yellow region on the graph), a new bubble is generated and the bubble recoil mechanism repeats. In the same solution, CBMs can also self-propel by double bubbles, as shown in Figure 3e. In this mode of propulsion, each new generated O_2 bubble collides with the previous one, leading to a larger step of motion of 8.8 µm. Typically, chemical compositions and the rate of decomposition of

fuels have a significant influence on the appearance of multiple connected bubbles. For instance, in a similar study, an addition of surfactant to hydrogen peroxide leads to a generation of long bubble trains by catalytic microtubes.[13,14] Some fraction of bubbles have holes, defects, or openings developed during drying step.[30] Figure 3f indicates individual CBM with O_2 microbubble generated from the gas core through an opening in the shell. In the latter case, the O_2 bubbles are connected during growth by the neck to the air core that remains stable in the nanoparticle-shelled bubble. Such CBMs self-propel both during O_2 bubble growth and ejection, leading to an average step of 11 µm. It is known that bubbles begin to appear on Janus micromotor with the diameter greater than 10 µm. Generally, a heterogenous bubble nucleation on catalytic surfaces depends on the O_2 saturation concentration and the curvature of the surface. Previously, Huang and co-workers investigated catalytic nanoshell micromotors (with internal Pt layer), where the bubble formation took place on the inner concave catalytic surface.[15] Bubbles require less energy to form on a flat solid surface than on a convex surface and even less energy on a concave surface. As a result, shell-like micromotors with catalyst coated inside the concave surface can achieve higher relative speeds. For instance, Huang and co-workers achieved 100 body length s^{-1} (concave catalytic shell, 2 µm diameter motor) and our nanoparticle-shelled bubbles self-propelled at 2 body length s^{-1} (convex catalytic shell, 170 µm diameter motor). It is noteworthy to mention that concave catalytic motors move faster than other types of convex motors.

Larger bubbles are known to induce an attractive capillary interaction due to the Cheerios effect at the water–air interface. However, nanoparticle-shelled microbubbles are not large enough to cause the monopolar interactions in water

due to their small Bond number, i.e., the ratio of body forces (including gravity and buoyancy forces) to the surface tension, is very small ($B_o = 10^{-5}$ to 10^{-3}).[29] As a result, a quadrupolar interaction is taking place between the CBMs that is not strong enough to induce bubbles' assembly at the planar air–solvent interface. Previously, a sessile drop, i.e., a convex air–water interface, was used to assemble the microbubble raft using buoyancy.[30] To attract microbubbles, a meniscus is created by inserting a glass capillary into the air–solution interface (Video S2, Supporting Information). Bond number for the bubbles themselves is small, but the glass capillary induces an attraction and assembly of bubbles due to macroscopic deformation of the meniscus (bubble does not induce a monopolar deformation, but glass capillary does). In our study, a microbubble raft is formed at the planar air–solvent (PC) interface induced by glass capillary, i.e., in the middle of Petri dish. The bubble raft is formed by the buoyancy of the bubbles and macroscopic deformation of the meniscus. The phenomenon of capillary curvature attraction is now well established, in prior work it was reported how interface curvature influence an attraction of microparticles.[31,32] An assembly of unmodified SiO_2 and amphiphilic Janus microbubbles showed strikingly different behaviors at a convex air–water interface.[33] Janus colloids can have undulating contact lines at the air–water interface and develop regions of attraction and repulsion among bubbles.[30] In our current study, new i) nonaqueous PC solvent and ii) a mixture of PC and aqueous hydrogen peroxide (chemical fuel) were used. Nanoparticle-shelled bubbles remain in stable static bubble rafts at the planar air–solvent (PC) interface and when H_2O_2 fuel is added bubbles break free from the bubble raft geometries. **Figure 4**a illustrates interactions acting on two bubbles, where F_b is the buoyancy force and F_w is weight of CBM. Figure 4b shows an optical microscopy image of assembled SiO_2-Ti/Pt microbubbles. Accepting

the diameter 150 µm, the shell thickness 3.1 µm, silica glass density 2200 kg m^{-3}, and gas density 1 kg m^{-3}—the weight of a hollow bubble is estimated on the order of 2.7×10^{-12} N. In contrast to gas-cored micromotors, other types of homogenous micromotors with a similar size could not self-propel due to a large weight to buoyancy ratio.

Upon an addition of H_2O_2 fuel to PC, bubble rafts break and CBMs start self-propelling at the air–solution interface. Figure 4c illustrates optical microscopy images and trajectories of motion of a) single, b) double, c) triple, d) quadruple, and e) nonuple CBMs (Video S3, Supporting Information). Here, the observed bubbles' clusters are connected by thin metallic films during the e-beam evaporation. These connected bubbles are different from assembled bubbles shown in Figure 4b, where CBMs are possibly hold together by other short-range interactions. Figure 4d,e shows a schematic and optical microscopy images of the dynamic assembly of CBMs using capillary force. A rapid disassembly of CBMs is taking place upon an addition of hydrogen peroxide to PC (Video S4, Supporting Information), Figure 4f (H_2O_2: $c_1 = 3.5\%$ v/v, $c_2 = 7\%$ v/v, $c_3 = 10.5\%$ v/v). Previously, a similar dynamic behavior was observed for bubble-propelled meniscus-climbing bubble-propelled microtubes.[34]

In our approach, stable compound microbubbles based on the air-in-oil-in-water (A/O/W) emulsions are generated using microfluidic techniques, followed by Ti/Pt catalyst e-beam deposition. Gas-cored micromotors form static bubble rafts at the air–solvent interface, while an addition of aqueous hydrogen peroxide fuel leads to a disassembly of bubble rafts and micromotors' self-propelled motion. Further study can provide new insights into interactions among nanoparticle-shelled bubbles in complex chemical fuels. By combining different modes of motility with methods of external control can enable unprecedented accuracy to position microbubbles for a
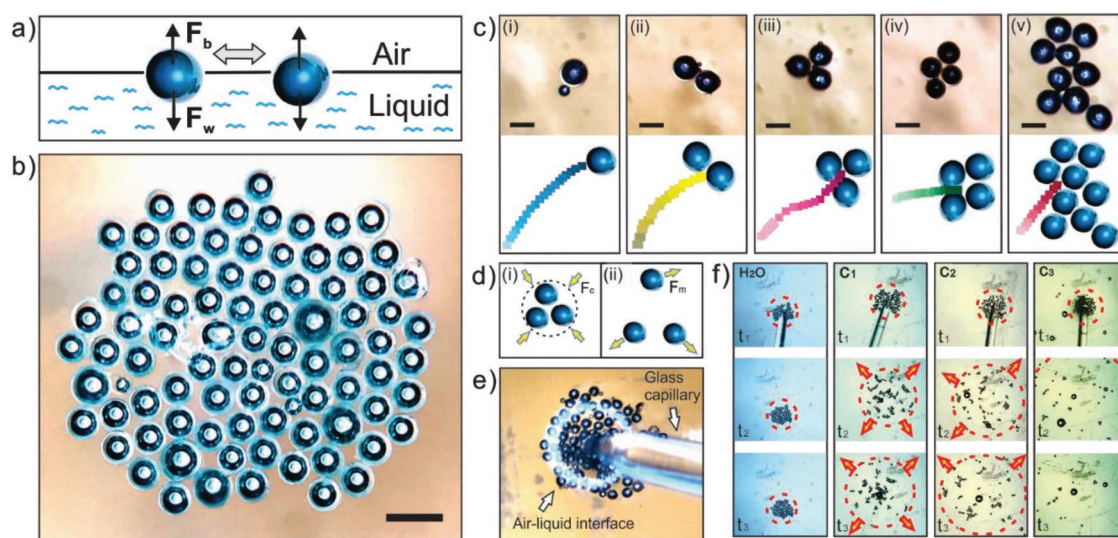
Figure 4. Static and dynamic interactions of microbubbles at the fuel/solvent–air interface. a) Schematic illustration of two separated bubbles, balanced by buoyancy (F_b) and weight (F_w). b) Optical microscopy image of the microbubble raft at the air–PC interface. The scale bar is 300 µm. c) Optical microscopy images (i–v) and schematic illustrations of self-propelled micromotors' clusters. The scale bar is 150 µm. d) A schematic of a dynamic bubble cluster, where competing attractive (F_c) and motive (F_m) forces are indicated by arrows. e) Optical microscopy image represents an assembly of micromotors induced by the capillary force, i.e., an external glass capillary inserted at the air–solution interface. f) Optical microscopy image showing sequences of static (in PC solvent) and dynamic assemblies of micromotors in different concentrations of H_2O_2 fuel in PC during 2 min ($t_1 - t_3$).

specific application. For instance, monodisperse microbubbles consisting of stable shells with desired mechanical, chemical, physical, and biomedical properties can potentially be used in both ultrasound-driven noninvasive imaging and targeted drug delivery techniques. In future, bioactive microbubbles can combine other types of catalysts, which exhibit enzyme-like characteristics.

Conflict of Interest

The authors declare no conflict of interest.

[1] J. Wang, *Nanomachines: Fundamentals and Applications*, Wiley-VCH, Weinheim, Germany **2013**.
[2] H. Zhu, S. Nawar, J. G. Werner, J. Liu, G. S. Huang, Y. F. Mei, D. A. Weitz, A. A. Solovev, *J. Phys.: Condens. Matter* **2019**, *31*, 214004.
[3] W. Wang, W. Duan, S. Ahmed, T. E. Mallouk, A. Sen, *Nano Today* **2013**, *8*, 531.
[4] H. Ning, Y. Zhang, H. Zhu, A. Ingham, G. S. Huang, Y. F. Mei, A. A. Solovev, *Micromachines* **2018**, *9*, 75.
[5] X. Ma, H. Feng, C. Liang, X. Liu, F. Zeng, Y. Wang, *J. Mater. Sci. Technol.* **2017**, *33*, 1067.
[6] F. Mou, C. Chen, Q. Zhong, Y. Yin, H. Ma, J. Guan, *ACS Appl. Mater. Interfaces* **2014**, *6*, 9897.
[7] W. Duan, W. Wang, S. Das, V. Yadav, T. E. Mallouk, A. Sen, *Annu. Rev. Anal. Chem.* **2015**, *8*, 311.
[8] M. Safdar, J. Simmchen, J. Jänis, *Environ. Sci.: Nano* **2017**, *4*, 1602.
[9] H. Eskandarloo, A. Kierulf, A. Abbaspourrad, *Nanoscale* **2017**, *9*, 13850.
[10] W. Gao, X. Feng, A. Pei, Y. Gu, J. Li, J. Wang, *Nanoscale* **2013**, *5*, 4696.
[11] F. Mou, D. Pan, C. Chen, Y. Gao, L. Xu, J. Guan, *Adv. Funct. Mater.* **2015**, *25*, 6173.
[12] J. Parmar, D. Vilela, K. Villa, J. Wang, S. Sánchez, *J. Am. Chem. Soc.* **2018**, *140*, 9317.
[13] A. A. Solovev, Y. Mei, E. Bermúdez Ureña, G. Huang, O. G. Schmidt, *Small* **2009**, *5*, 1688.
[14] Y. Mei, G. Huang, A. A. Solovev, E. B. Ureña, I. Mönch, F. Ding, T. Reindl, R. K. Y. Fu, P. K. Chu, O. G. Schmidt, *Adv. Mater.* **2008**, *20*, 4085.
[15] W. Huang, M. Manjare, Y. Zhao, *J. Phys. Chem. C* **2013**, *117*, 21590.
[16] M. Safdar, T. Itkonen, J. Jänis, *RSC Adv.* **2015**, *5*, 13171.
[17] Y. Wu, Z. Wu, X. Lin, Q. He, J. Li, *ACS Nano* **2012**, *6*, 10910.
[18] L. Wang, Y. Liu, J. He, M. J. Hourwitz, Y. Yang, J. T. Fourkas, X. Han, Z. Nie, *Small* **2015**, *11*, 3762.
[19] B. A. Grzybowski, K. Fitzner, J. Paczesny, S. Granick, *Chem. Soc. Rev.* **2017**, *46*, 5647.
[20] J. Zhang, E. Luijten, B. A. Grzybowski, S. Granick, *Chem. Soc. Rev.* **2017**, *46*, 5551.
[21] A. Nourhani, D. Brown, N. Pletzer, J. G. Gibbs, *Adv. Mater.* **2017**, *29*, 1703910.
[22] P. Bayati, A. Najafi, *J. Chem. Phys.* **2016**, *144*, 134901.
[23] Y. Gao, F. Mou, Y. Feng, S. Che, W. Li, L. Xu, J. Guan, *ACS Appl. Mater. Interfaces* **2017**, *9*, 22704.
[24] J. J. Palacci, S. Sacanna, A. Preska Steinberg, D. J. Pine, P. M. Chaikin, *Science* **2013**, *339*, 936.
[25] B. A. Grzybowski, H. A. Stone, G. M. Whitesides, *Nature* **2000**, *405*, 1033.
[26] T. Xu, F. Soto, W. Gao, R. Dong, V. Garcia-Gradilla, E. Magaña, X. Zhang, J. Wang, *J. Am. Chem. Soc.* **2015**, *137*, 2163.
[27] M. H. Lee, V. Prasad, D. Lee, *Langmuir* **2010**, *26*, 2227.
[28] T. Brugarolas, F. Tu, D. Lee, *Soft Matter* **2013**, *9*, 9046.
[29] Y. Zhang, H. Zhu, W. Qiu, Y. Zhou, G. S. Huang, Y. F. Mei, A. A. Solovev, *Chem. Commun.* **2018**, *54*, 5692.
[30] T. Brugarolas, B. J. Park, M. H. Lee, D. Lee, *Adv. Funct. Mater.* **2011**, *21*, 3924.
[31] I. B. Liu, G. Bigazzi, N. Sharifi-Mood, L. Yao, K. J. Stebe, *Phys. Rev. Fluids* **2017**, *2*, 100501.
[32] I. B. Liu, N. Sharifi-Mood, K. J. Stebe, *Annu. Rev. Condens. Matter Phys.* **2018**, *9*, 283.
[33] L. C. Bradley, W.-H. Chen, K. J. Stebe, D. Lee, *Curr. Opin. Colloid Interface Sci.* **2017**, *30*, 25.
[34] A. A. Solovev, Y. F. Mei, O. G. Schmidt, *Adv. Mater.* **2010**, *22*, 4340.